Two-Dimensional Aperiodic Flows in a Rectangle Subject to a Harmonic Forcing

Yong Kweon Suh*

(*Received July 15, 1996*)

An unsteady two-dimensional incompressible flow inside a rectangular container under a torsional oscillation has been numerically obtained. Effect of three parameters, the aspect ratio, the dimensionless angular frequency, and the Reynolds number, on the flow pattern's development is studied. The flow is irregular and aperiodic at the Reynolds number 5000.Some aspects of the vortical flow dynamics are investigated. Observed in the numerical experiment are stretching, folding, splitting, merging, and curling etc.

Key Words: Aperiodic Flow, Rectangle, Harmonic Forcing, Vortical Flow Dynamics

1. Introduction

This paper presents two-dimensional incompressible flow patterns inside a rectangular container under a torsional oscillation. Figure 1 is a schematic illustration of the container shape and the way it oscillates. This flow model is in fact similar to that studied by van Heijst, Davies, and Davis(1990) and Suh(1994) as a spin-up process; the only difference lies in that they considered the suddenly and then uniformly rotating case, whereas here the container rotates back and forth in a sinusoidal mode.

While in the spin-up process the flow decays after some finite time, in the sinusoidal forcing like the present study it never decays. The flow patterns also undergo more complicated and diverse development in this model. In view of symmetric properties of both the container geometry (spatial symmetry) and the forcing term (temporal symmetry), it is relevant to concentrate on whether the flow also preserves the symmetry as paremeter values are varied. At low Reynolds number, the flow keeps the spatial as well as temporal symmetry. At higher Reynolds number, it is broken both spatially and temporally. The flow field thus becomes neither regular nor periodic.

The final goal of this study is to develop some theoretical or numerical tools for analysis of the stirring of aperiodic or turbulent flows; tools such as the Poincare section and the unstable manifold developed for the periodic two-dimensional or steady three-dimensional flow may not be applicable to aperiodic flows (e. g. Aref, 1984 and Ottino, 1989). In this paper, however, we focuss our attention on the flow field only.

In §2, the flow model is formulated and the numerical methods are briefly explained. Symmetry properties are analysed in §3. §4 presents the numerical results. The effect of three parameters, the aspect ratio, the angular frequency, and the Reynolds number on the flow development is separately considered. We summarize the important findings in §5.

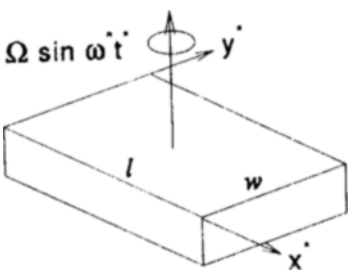

Fig. 1 A rectangular container containing a fluid subject to a horizontal angular oscillation.

* Department of Mechanical Engineering, Dong-A University Pusan 604-714, Korea

2. Formulation and Numerical Method

Scaling the lengths by w, the time by $1/\Omega$, and the velocities by $w\Omega$, we can write the dimensionless governing equations as

$$\frac{\partial \zeta}{\partial t}+\frac{\partial \psi}{\partial y}\frac{\partial \zeta}{\partial x}-\frac{\partial \psi}{\partial x}\frac{\partial \zeta}{\partial y}=\frac{1}{Re}\nabla^2\zeta+2\cos\omega t \quad (1)$$

$$\nabla^2\psi=\zeta \quad (2)$$

where ∇^2 is the Laplacian operator, t is the dimensionless time, (x, y) is a dimensionless coordinate system moving with the container, ψ is the dimensionless streamfunction, ζ is the dimensionless vorticity, ω is the dimensionless angular frequency given by

$$\omega=\frac{\omega^*}{\Omega} \quad (3)$$

and Re is the Reynolds number defined as

$$Re=\frac{w^2\Omega}{\nu} \quad (4)$$

where ν is the kinematic viscosity of the fluid. The origin of the coordinates (x, y) is at one corner of the container, and x and y are along the long and short sides, respectively.

The initial values for ζ and ψ are set zero. Along the four sides of the rectangle, the no-slip condition is applied;

$$\psi=\frac{\partial \psi}{\partial n}=0, \text{ at } x=0,\ a \text{ and } y=0,\ 1 \quad (5)$$

where n is along the normal direction at each boundary, and

$$a=\frac{l}{w} \quad (6)$$

is the aspect ratio.

We construct a grid system with J×K meshes for the entire domain for the spatial discretization. The central difference is used for all the spatial derivatives in the equations and the integration of (1) over the time is performed by using the forth-order Runge-Kutta method. The Poisson equation, Eq. (2), is integrated by the line SOR method. Detailed numerical methods and procedure are given in Suh (1994, 1997) and will not be repeated here.

3. Symmetry Properties

We expect intuitively that the solution can be antisymmetric with respect to the center point $(a/2, 1/2)$. Indeed, in the governing Eqs. (1) and (2), replacing $\psi(x, y, t)$ by $\psi(a-x, 1-y, t)$ and $\zeta(x, y, t)$ by $\zeta(a-x, 1-y, t)$ does not alter the original operators. This fact supplemented by the geometrical symmetry (boundary-condition symmetry) guarantees the antisymmetric nature of the solutions;

$$\psi(x, y, t)=\psi(a-x, 1-y, t) \text{ and}$$
$$\zeta(x, y,)=\zeta(a-x, 1-y, t) \quad (7)$$

On the other hand, regarding the temporal structure, we can also assume one of the following properties; either

$$\psi(x, y, t)=-\psi(a-x, y, t+T/2) \text{ and}$$
$$\zeta(x, y, t)=-\zeta(a-x, y, t+T/2) \quad (8a)$$

or

$$\psi(x, y, t)=-\psi(x, 1-y, t+T/2) \text{ and}$$
$$\zeta(x, y, t)=-\zeta(x, 1-y, t+T/2) \quad (8b)$$

where $T=2\pi/\omega$ is the dimensionless period. If the spatial antisymmetric nature is simultaneously satisfied, the above two properties are not independent.

We will see from the numerical results in the next section that at low Reynolds numbers, these properties are indeed preserved, but we will also see that the symmetry properties are lost at high Reynolds numbers.

4. Numerical Results and Discussions

In the present numerical experiment at high Reynolds numbers, the numerical instability seems to be sensitive more to the spatial resolution, that, is $\triangle x=\triangle y=1/(K-1)$ than to the time step $\triangle t=2\pi/\omega N$. For instance, for $a=3$, $\omega=0.4$, and $Re=5000$, the mesh system $J\times K=241\times 81$ shows instability after 2 periods for both $N=1600$ and 2400, while the mesh system $J\times K=301\times 101$ is successful upto 10 periods for $N=1600$.The instability is also affected by a. For $a=4$, $\omega=0.4$, and $Re=5000$, the mesh system $J\times K$

Table 1 Parameter values for 7 cases of numerical experiment. M is the number of periods of calculation.

Cases	a	ω	Re	$J\times K$	N	M
A	1	0.4	5000	101×101	2400	30
B	2	0.4	5000	201×101	2400	20
C	3	0.4	5000	361×121	2400	15
D	2	0.4	500	201×101	2400	20
E	2	0.4	1500	201×101	2400	20
E	2	0.2	5000	201×101	4800	15
G	2	1.0	5000	241×121	1200	15

$=401\times 101$ shows instability after 2 periods for $N=1600$. On the contrary, for $a=1$, $\omega=0.4$, and $Re=5000$, the mesh system $J\times K=101\times 101$ is successful upto 30 periods for $N=2400$. It is conjectured that the instability is caused by the stronger vortex motion at higher aspect ratios.

Three physical parameters to be studied are a, the aspect ratio, ω, the dimensionless angular frequency, and Re, the Reynolds number. Table 1 shows 7 sets of parameter values that are used in obtaining the numerical solutions.

4.1 Effect of a

With $\omega=0.4$ and $Re=5000$, three values of a are used in studying the effect of a (cases A, B, and C in Table 1). Figure 2 shows evolution of streamline and vorticity patterns for the last one period of the case A. Let's first look into the vorticity pattern. During the first half period, $0\leqq t\leqq T/2$, four positive vortices ('white' in the figure) generated near four corners are merged in the core. At the end of the first half period (at $t=T/2$), four negative vortices ('black' in the figure) are generated near the same corners. These vortices are then merged during the latter half period in the core. Referring to Fig. 2(a), we see that the flow is almost clockwise during the first half period and anticlockwise during the second half period. The flow is almost stagnant at the intermediate times, i. e. at $t=0$, $T/2$, and T. This indicates that, for this case, the flow is almost anticyclonic (rotating in a direction opposite to the container's motion; refer to e. g. Lugt, 1983). We further note that the antisymmetric property (7) is present.

For the flow to be periodic, the pattern at $t=0$ must be the same as that at $t=T$. It is interesting to note from Fig. 2 that one pattern can be reproduced by turning the other as much as 90° angle. The temporal periodicity can be detected by the spatial-average quantity $\bar{\psi}$ defined as

$$\bar{\psi}(t)=\frac{1}{A}\int_A \psi dA$$

where A is the area of the entire flow field. As shown in Fig. 3, the case of $a=1$ yields a periodic function $\bar{\psi}$, which tentatively predicts that the pattern may be periodic. This figure further shows that at $a=2$ and 3, the flows must be aperiodic.

Shown in Figs. 4 and 5 are streamline and vorticity patterns for $a=2$ and 3, respectively, during the final period of computation. Indeed, the flow patterns at $t=0$ are not reproduced at $t=T$. Moreover, no symmetry properties in the flow patterns are observable for these cases. So, the flows are neither ordered nor periodic. We see that the patterns (especially the vorticity pattern) are so much complicated in structure and the pattern's evolution is hardly understandable. However we can pick up the most notable and common feature; an interior cell generates a vorticity of opposite sign near the touching boundaries, which after assembled becomes another cell of comparable size (e. g. the region near the boundary $x=2$ during the first half period in Fig. 4).

By comparing the two cases, we can understand some distinctive features in each pattern's development. For the case of $a=2$ (Fig. 4), the flow solution can be characterized by competition between two-cell structure and three-cell structure. At $t=0$ the field is composed of three cells. The central anticlockwise cell is then stretched,

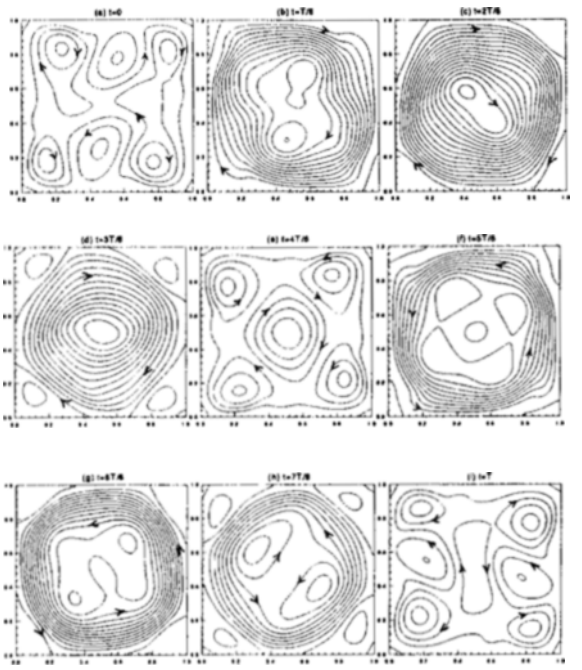

(a) The streamline patterns

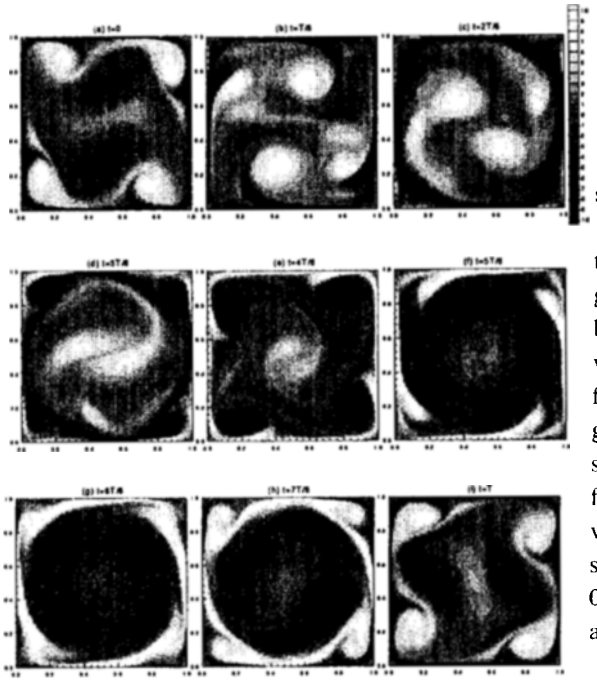

(b) The vorticity patterns

Fig. 2 Streamline patterns (a) and the vorticity patterns (b) for $a=1$, $\omega=0.4$, and $Re=5000$ (case A). The increment of the stream function in (a) is 0.01. These plots are for the last one (30th) period.

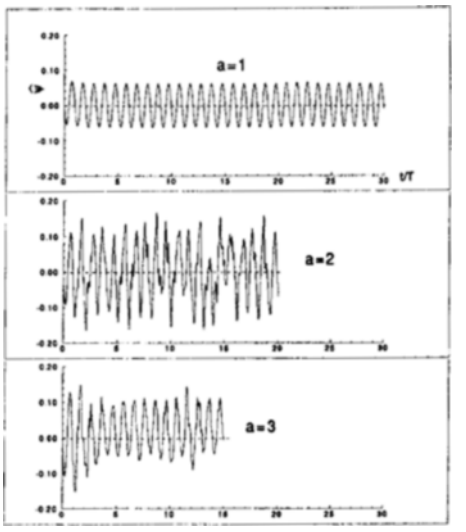

Fig. 3 History of $\tilde{\phi}$ for three values of a shown (cases A, B, and C from above); $\omega=0.4$, $Re=5000$.

splitted, and disappears, resulting in a two-cell structure at $t=2T/8$. After this instant, however, another anticlockwise cell is generated near the left-bottom corner and then moves to the interior region yielding a three-cell structure at $t=4T/8$. From this time, the clockwise cell at the righthand side undergoes a similar process giving two-cell (at $t=5T/8$) and three-cell ($t=6T/8$) structures. During the entire course, some cells are growing by being fed with the vorticity generated by the neighboring opposite cells and some are weakened by being stretched and splitted into a few parts by the action of the neighboring cells. In general, we can say that the central cell corresponds to the latter, while the side cells to the former. A typical feature in the dynamics of vorticity blobs is 'folding'; for instance, a vertical streak of negative vorticity shown at $x\cong 1.8$ at $t=0$ in Fig. 5 is folded at $t=T/8$. We can also see a lot of such folded structures in Figs. 4 and 5.

For the case of $a=3$ (Fig. 5), the cell structure is slightly more stable than the case of $a=2$ ('stable' in the sense that each cell tends to keep its position). The flow field is characterized by a four-cellstructure during the first half period and three-cell structure during the second half period. For the whole period, two cells at the lefthand

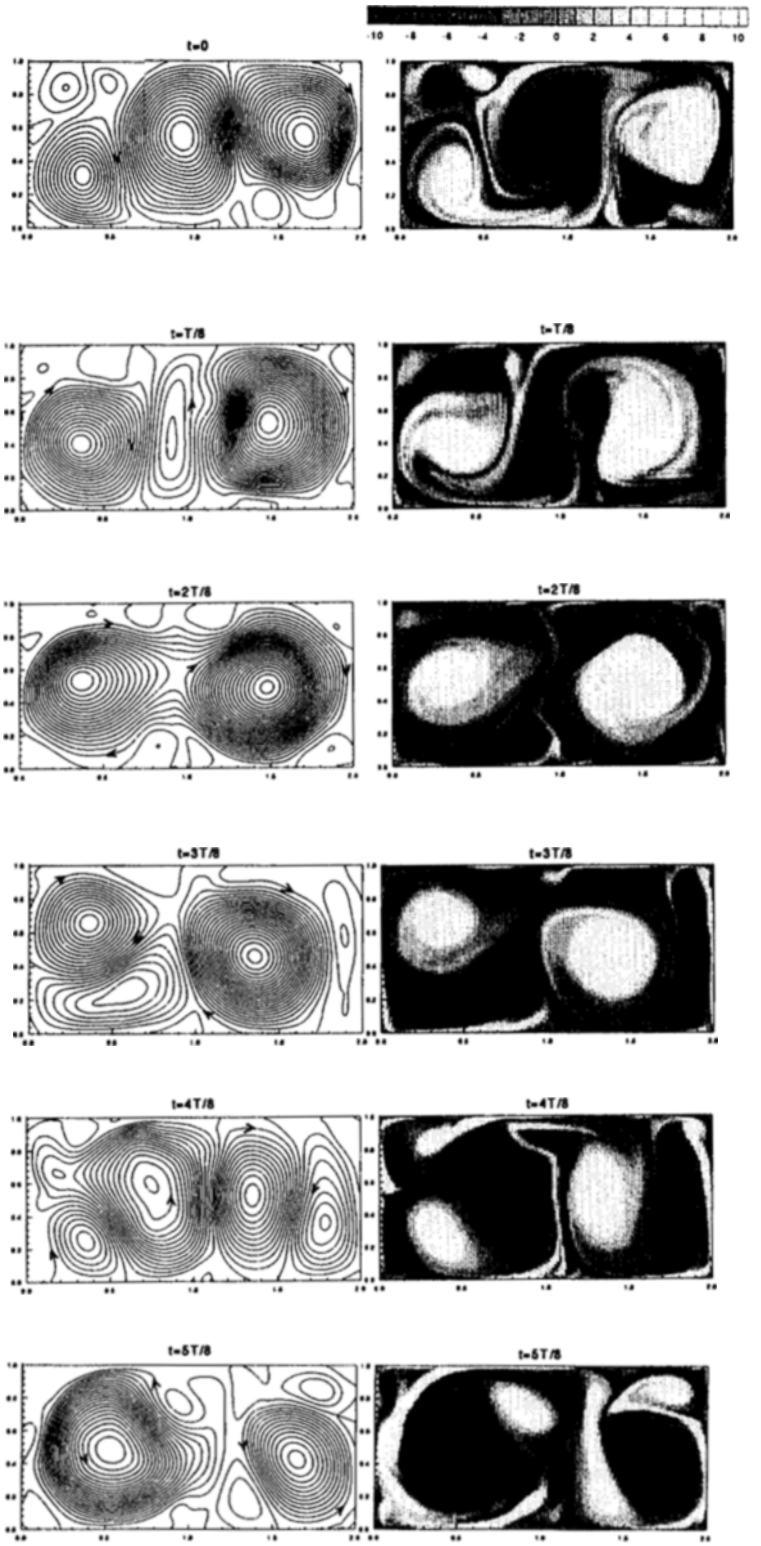

(**Fig. 4** Continued)

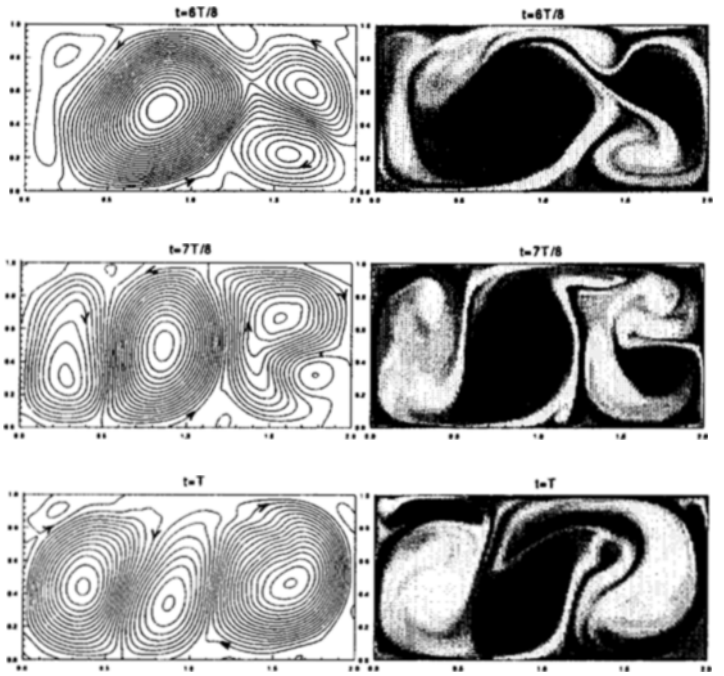

Fig. 4 Streamline and vorticity patterns for $a=2$, $\omega=0.4$, and $Re=5000$ (case B). The increment of the stream function is 0.02. These plots are for the last one (20th) period.

side region keep each position, and when one grows the other shrinks, and vice versa. The cells at the righthand side are, however, suffering a rather catastrophic event. At the first stage ($t \leq 2T/8$), the anticlockwise cell situated to the interior is shrinked and the clockwise cell is enlarged. The continuous feeding of the negative vorticity generated near the upper boundary makes the anticlockwise cell grow and finally moves through the upper boundary the clockwise cell to its lefthand side. The moved vortex then merges with the central clockwise vortex, making it the biggest among three ($t=T$).

If the flow field were composed of four cells of equal size, then $\bar{\psi}=0$, and if it were composed of three cells of equal size, then $\bar{\psi}>0$ when two are anticlockwise and $\bar{\psi}<0$ when they are clockwise. Thus, referring to the history of $\bar{\psi}$ in Fig. 3, we can see that the case of a=3 is characterized by competition between four-cell and three-cell structures, where two of them are anticlockwise. This figure also illustrates that the case of $a=2$ is more aperiodic than $a=3$; in fact we can see a larger variation of the local maximum or minimum of $\bar{\psi}$ for $a=2$.

Figure 6 shows the time-average streamline patterns (steady streaming motion) obtained from $\bar{\psi}(x, y)$ defined as

$$\bar{\psi}(x, y)=\frac{1}{mT}\int_{nT}^{(n+m)T}\psi(x, y, t)\,dt$$

where n and m are integers. This figure shows results with $m=1$.We note that the steady motion is weakest for $a=1$ and strongest for $a=3$. The case of $a=2$ is significantly different if larger m is used as shown in Fig. 7. This indicates that while the case of $a=3$ has a persistent steady motion, that of $a=2$ has no appreciable steady motion.

4.2 Effect of Re and ω

As may be intuitively expected, the flow pattern is both ordered and periodic at low Reynolds numbers. Figure 8 is the numerical result for $a=2$, $\omega=0.4$, and $Re=500$. The flow field represents a two-cell structure composed of two clockwise cells at $t=0$, and becomes a one-cell structure at $t=T/8$. This cell then generates negative vorticity from both upper and lower boundaries.

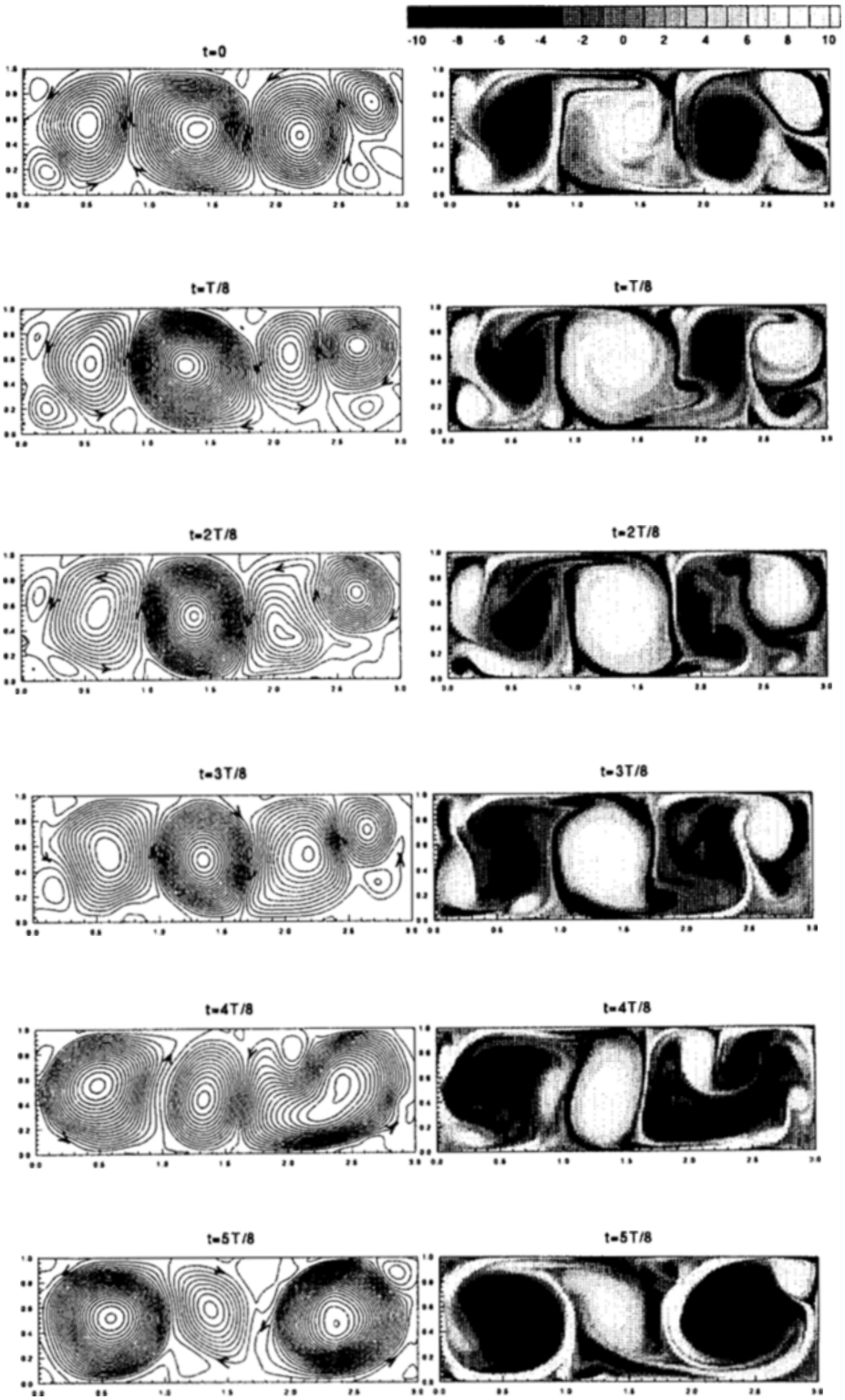

(Fig. 5 Continued)

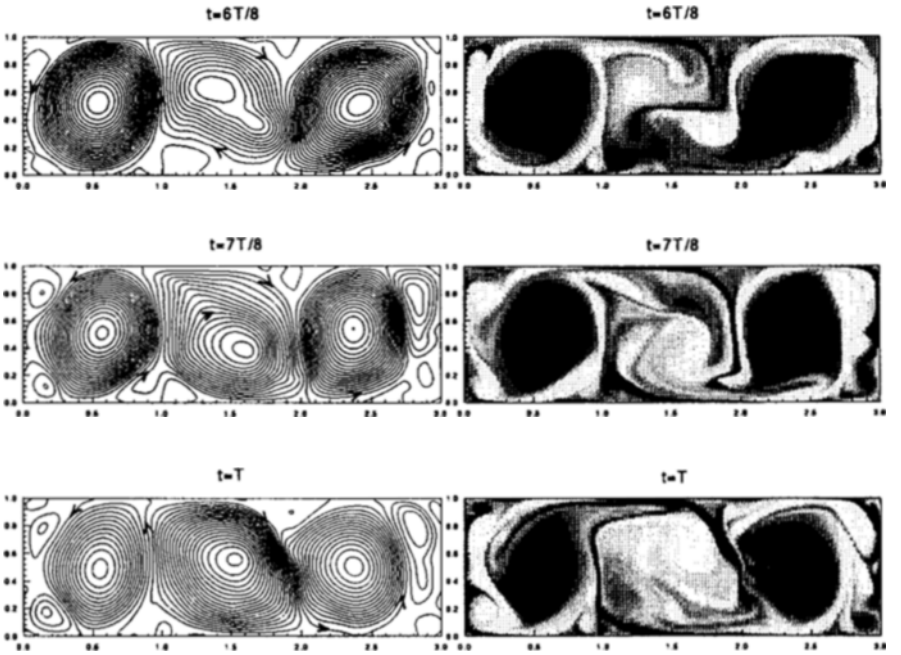

Fig. 5 Streamline and vorticity patterns for $a=3$, $\omega=0.4$, and $Re=5000$ (case C). The increment of the stream function is 0.02. These plots are for the last one (15th) period.

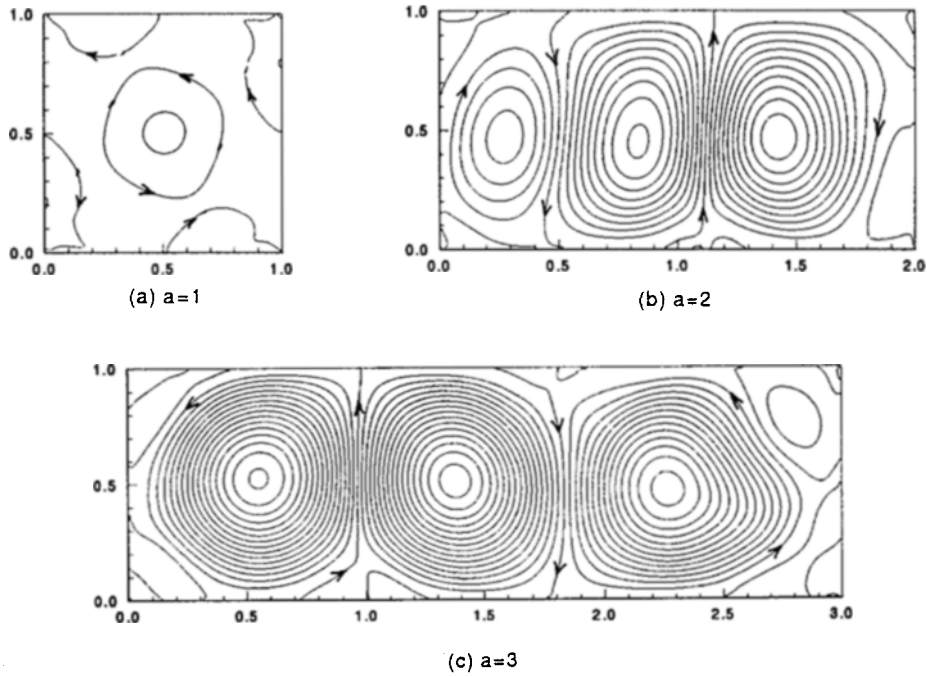

Fig. 6 Steady streamline patterns for three values of a shown; $\omega=0.4$, and $Re=5000$. The increment of the stream function is 0.02. These plots are for the last one period ($m=1$).

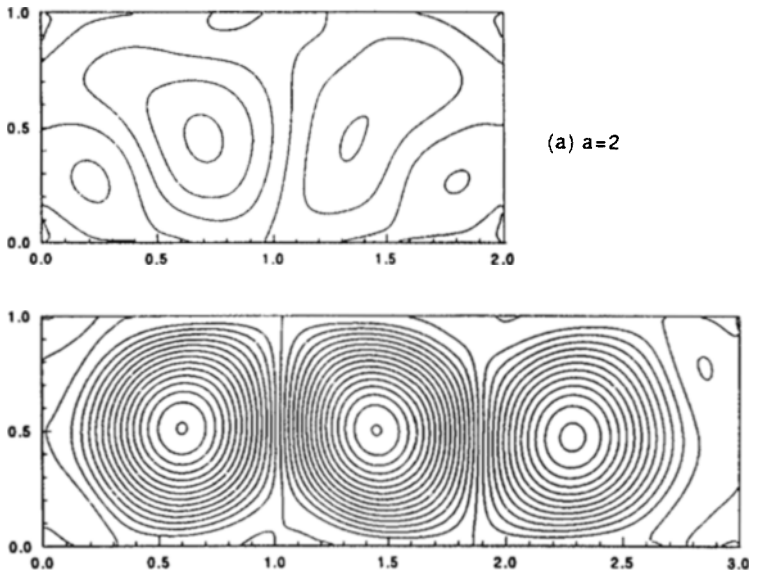

Fig. 7 Steady streamline patterns for two values of a shown; $\omega=0.4$, and $Re=5000$. The increment of the stream function is 0.02. These plots are for the last ten periods ($m=10$).

Accumulation (curling) of this vorticity at two sides produces two anticlockwise cells resulting in a three-cell system ($t=3T/8$). The central cell then disappears and simultaneously the two cells are merged to become a one-cell system ($t=5T/8$). The procedure following is similar to the previous one. We can see that for this case, both the geometrical and temporal symmetric properties (that is, (7) and either (8a) or (8b)) are preserved. The solution is also obtained for $Re=1500$, but the pattern's evolution is qualitatively the same as $Re=500$.

The effect of ω on the pattern's development is further studied. At lower ω, T is large so we can say that each vortex has enough time in its development. As a consequence, the cell pattern is less complicated than that of higher ω. At $\omega=1$ (classified as high ω value), the switching time between generation of positive and negative vorticity is so small that each vortex generated near the boundaries is of small size. Some of these vortices are merged with each other to become a regular-size cell, whereas others are for some while meandering as solitary cells. As a result the flow pattern looks more complicated and irregular than that of lower ω. We can of course expect an anticyclonic flow at higher ω. In this case, Eq. (1) gives the solution $\zeta=(2/\omega)\sin\omega t$, upon which ψ takes a separable form, $\psi=F(x, y)\sin\omega t$.

Steady streaming plots shown in Fig. 9 reveal three symmetry properties. At low Re, the pattern is symmetric with respect to both $x=a/2$ and $y=1/2$ (Fig. 9(a)). At low ω, the pattern tends to be symmetric with respect to $x=a/2$ (Fig. 9(b)), and at high ω, the symmetric property is not appreciable (Fig. 9(c)). We also note that the last case shows the weakest steady motion. Effect of the steady motion on the stirring is not clear at this moment, and it is remained as a future study.

4.3 Further discussions

We have seen that for $a=3$ the flow pattern is persistent and coherent. This implies that the cell structure is stable in a certain sense. To understand the stability mechanism, we first resort to the quasi-steady flow of a spin-up model (van Heijst et al, 1990 and Suh, 1994). In order to explain a critical phenomenon in the evolution of cell structures, Suh (1994) has studied the devel-

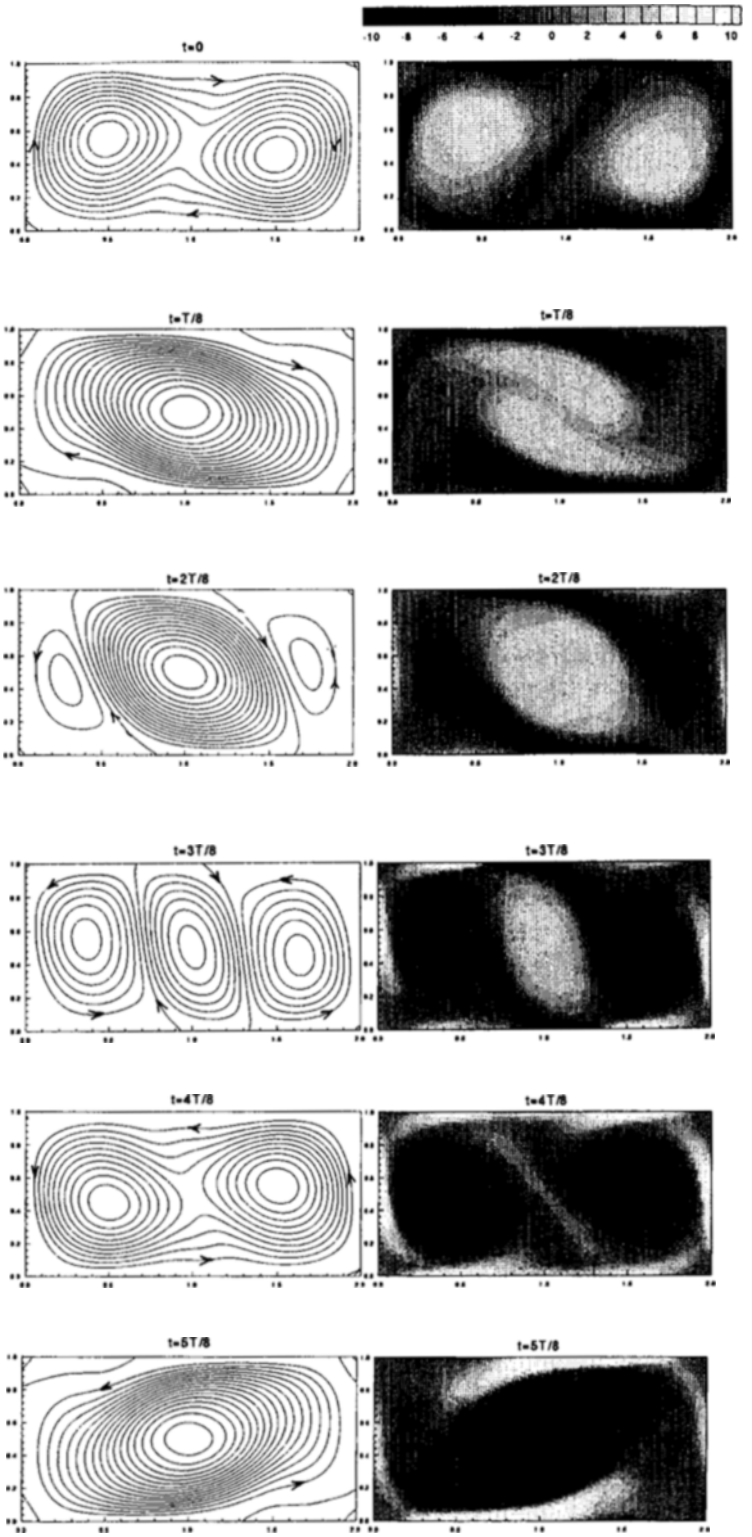

(Fig. 8 Continued)

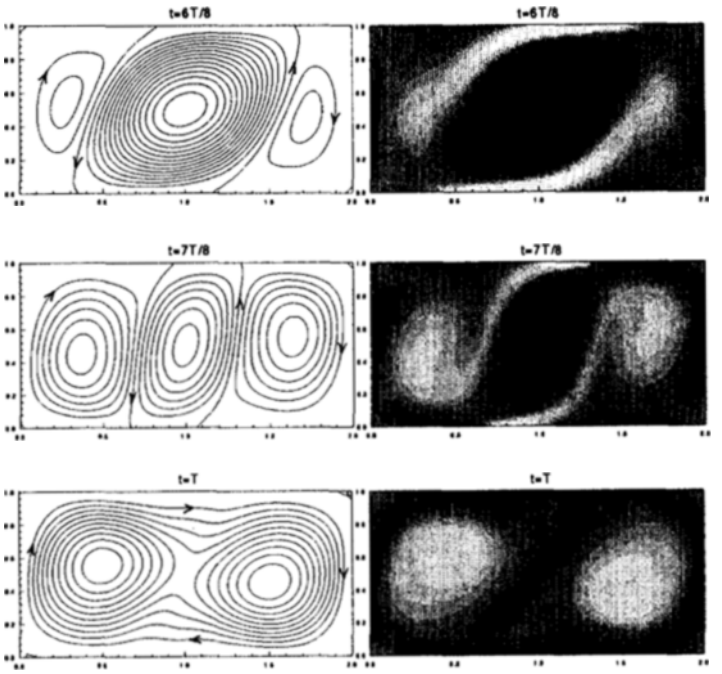

Fig. 8 Streamline and vorticity patterns for $\alpha=2$, $\omega=0.4$, and $Re=500$ (case D). The increment of the stream function is 0.02. These plots are for the last one (20th) period.

opment of a cellular flow in a rectangle of $\alpha=3$ initially composed of two large clockwise cells and one small central cell in between them as sketched in Fig. 10(a). He has numerically shown that there exists a critical width of the central cell at which a slightly larger width results in an eventually growing of the central cell while a slightly smaller width makes the central cell disappeared. Fig. 10(b) corresponds to the former case. The central cell is continuously fed with negative vorticity from the left-top and right-bottom boundaries induced by the two large vortical flows. This process ultimately leads to a structure of three cells of almost equal size.

Now we consider the present model (Fig. 5). As seen from Eq. (1), the whole flow field receives vorticity in a rate $2\cos\omega t$ (recall that the quasi-steday state of the spin-up model has no such body forces). Therefore during a half period ($-T/4\leq t\leq T/4$) it receives vorticity as much as $4/\omega$, and $-4/\omega$ during the latter half period. Receiving positive vorticity in turn tends to make the clockwise cell bigger and the anticlockwise smaller, and vice versa. However this repetitive vorticity supply is not enough to break the coherent structure present in the lefthand side of Fig. 5. It is abrupt to assume that a smaller ω causing a larger vorticity supply can break this structure.

On the other hand, we can of course expect an equal chance of obtaining an opposite flow structure by changing the initial conditions. For instance we can obtain a flow structure that gives a time series of $\tilde{\phi}$ symmetric with respect to the t-axis of Fig. 3 for $\alpha=3$ by starting the computation from $t=T/2$ not $t=0$; this is mathematically guaranteed by the fact that the governing equations are invarient under the transformation (8a) or (8b). Consequently, the given solution can be chracterized as 'bistable'. These two stable structures are intuitively conjectured to be 'broken' or 'connected' to each other when ω is small enough.

Understanding the complex evolution of a physical phenomenon in terms of a figuratively simple dynamical model is often very useful. Figure 11 shows the so called 'two-well potential' problem. An infinitesimal particle of finite mass slides on a surface moving sinusoidally in the

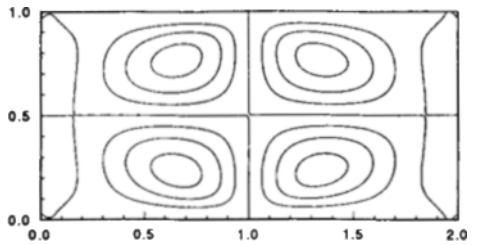

(a) ω=0.4, Re=500

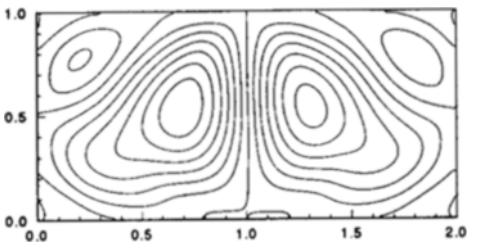

(b) ω=0.2, Re=5000

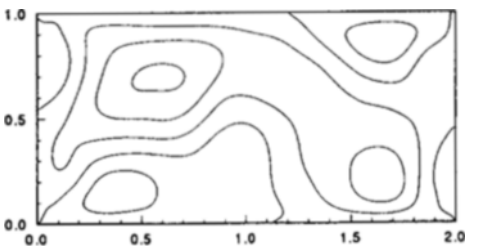

(c) ω=1.0, Re=5000

Fig. 9 Steady streamline patterns for three sets of parameters for $a=2$. The increment of the stream function is 0.01. These plots are for the last ten periods ($m=10$).

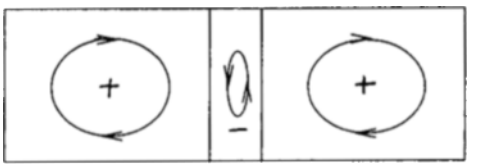

(a) Initial state

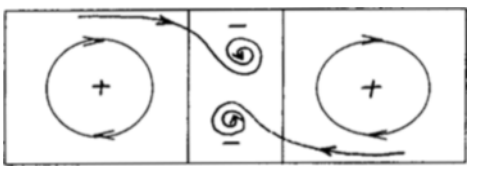

(b) Growing of the central cell

Fig. 10 Development of a three-cell flow structure inside a rectangle of $a=3$; the central cell being initially narrow.

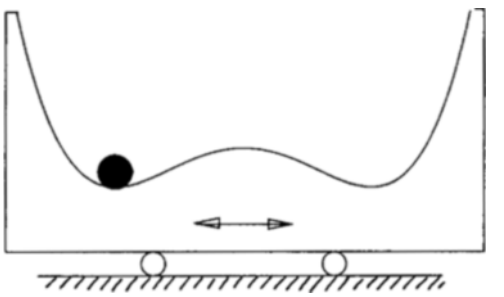

Fig. 11 Two-well potential system, where a particle (black circle) with infinitesimal size but finite mass slides on an oscillating surface having two wells.

horizontal direction. The equation governing the particle's motion is the Duffing equation and has been first studied extensively by Holmes (1979); see also the text by Moon (1987). This system is here purposed to serve as a figurative model that reveals some ingredients of the present hydrodynamical model. At a suitable parameter set, the particle can oscillate locally in the either left or right well depending on the initial conditions; in fact this is a typical example of bistable systems. On the other hand, the particle can oscillate globally visiting both sides in the same probability, if the frequency of the external forcing is small enough. These two properties (i. e. that the system is bistable and that the two stable motions are connected at a small frequency) are well representative of the present system. The third property of the two-well potential system is a critical phenomenon. For a parameter set at which the particle's motion is locally confined, a small change in the initial conditions can give the motion around the opposite well. The same phenomenon is conjectured to occur in the present flow system. A similar phenomenon has also been observed by Suh (1997) for the case of a two-dimensional oscillating-lid-driven-cavity problem.

5. Conclusions

The time evolution of vortical flow structures

inside a rectangle subject to a sinusoidal forcing has been numerically investigated. The parameter values for the base case (case B in Table 1) among the various sets are; $a=2$, $\omega=0.4$, and $Re=5000$. Three parameters are changed separately and the solution of each case is carefully examined. Some important findings can be summarized as follows.

(1) At high Reynolds numbers, the numerical instability cannot be overcome only by decreasing the time step; the spatial resolution must be increased.

(2) The flow pattern is almost periodic and anticyclonic at $a=1$, and the pattern becomes irregular and aperiodic at $a=2$ and 3.

(3) The case of $a=2$ can be characterized by competition between two-cell and three-cell structures. For $a=3$, the cell structure is slightly more stable than $a=2$ and it can be characterized by competition between three-cell and four-cell structures.

(4) At lower Reynolds numbers ($Re=500$ and 1500), the flow patterns develop regularly and periodically. The symmetry propeties are exactly preserved at these values of Re.

(5) At higher ω ($\omega=1$), the flow field is composed of many vortices of small size and resultantly the pattern apparently looks more complicated.

(6) Three dynamical properties of this system can be figuratively explained from the two-well potential problem.

Acknowledgement

The financial support of the Korea Science and Engineering Foundation (Grant No. 95-0200-06-01-3) is gratefully acknowledged.

References

Aref, H., 1984, "Stirring by Chaotic Advection," *J. Fluid Mech.* 143, 1~21.

Holmes, P. J., 1979, "A Nonlinear Oscillator with a Strange Attractor," *Phil. Trans. R. Soc. London* A 292, 419~448.

Lugt, H. J., 1983, *Vortex Flow in Nature and Technology*, John Wiley & Sons, p. 132.

Moon, F. C., 1987, *Chaotic Vibrations*, John Wiley & Sons.

Ottino, J. M., 1989, *The Kinematics of Mixing: Stretching, Chaos, and Transport*, Cambridge University Press.

Suh, Y. K., 1994, "Numerical Study on Two-Dimensional Spin-up in a Rectangle," *Phys. Fluids* 6 (7), 2333~2343.

Suh, Y. K., 1997, "Comparison of Multi-Stage Explicit Methods for Numerical Computation of the Unsteady Navier-Stokes Equations," *Trans.* KSME 21 (2), 202~212 (in Korean).

Van Heijst, G. J. F., Davies, P. A. and Davis, R. G., 1990, "Spin-up in a Rectangular Container," *Phys. Fluids* A 2, 150~159.